Cyclotron Detector Development for $\bar{\text{p}}$ Transport at BASE-STEP

Matthew Everette[1] and Christian Smorra[2]

[1]Clemson University
[2]Heinrich-Heine Universität Düsseldorf

August 2024

Abstract

In this report, I detail my development of a new cyclotron detector system for the BASE-STEP experiment. BASE-STEP seeks to transport antiprotons created at CERN to an off-site laboratory with a more stable magnetic field background – a current limitation of high-precision measurements conducted in CERN's AD hall. Currently, the cyclotron detectors in the BASE-STEP trap are highly coupled, harming their performance. The new cyclotron detector setup resolves this issue with a robust varactor board, providing a significant tuning range of ~540kHz at low operating temperatures. Moreover, the new resonator was designed to provide a higher inductance of $L = 3.7\mu\text{H}$, leading to a 25% reduction in the detector's cooling time constant τ.

1 Introduction

The Baryon-Antibaryon Symmetry Experiment (BASE) at CERN seeks to compare the properties of protons and antiprotons to high precision in order to test charge, parity, and time reversal (CPT) invariance in the universe and search for physics beyond the Standard Model. While observation leads us to believe that the universe is almost entirely made up of matter, current cosmological theory and the Standard Model of particle physics predict a roughly equal amount of matter and antimatter in the universe – a theoretical inconsistency known as the baryon asymmetry problem. In string theory, CPT violating processes provide a potential solution to the problem of baryon asymmetry [1]. High precision comparisons of particles and their antiparticles constitute stringent tests of CPT invariance, thus allowing us to perform low-energy searches for beyond the Standard Model physics.

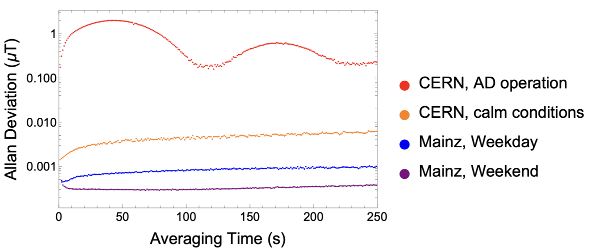

Figure 1: Comparison of the volatile background magnetic field at CERN's AD hall to the calm background field at a laboratory in Johannes Gutenberg-Universität Mainz. Reproduced from [2].

BASE conducts high-precision measurements of the charge-to-mass ratios of protons and antiprotons as well as the antiproton g-factor in CERN's Antiproton Decelerator (AD) hall. Antiprotons produced in the AD-hall are captured within the BASE collaboration's four Penning trap experimental setup, and subsequent measurements of a single particle's free cyclotron frequency ν_c and Larmor frequency ν_L are conducted. Currently, noise generated by the magnetic field of the AD, shown in Figure 1, is a limiting factor in further improving the precision of BASE's measurements. BASE-STEP (Symmetry Tests in Experiments with Portable antiprotons) is developing a transportable antiproton trap to transport antiprotons produced in the AD hall to a off-site laboratory with a more stable magnetic field background for even-higher-precision measurements [2].

1.1 Penning Traps

Both BASE and BASE-STEP use Penning traps to trap antimatter. When constrained inside a Penning trap, as shown in Figure 2, particles undergo three modes of oscillation: magnetron motion, axial motion, and modified cyclotron motion. The free cyclotron frequency of a particle in the trap can be determined using the frequencies of these different modes of oscillation through the invariance theorem:

$$\nu_c^2 = \nu_-^2 + \nu_z^2 + \nu_+^2$$

where ν_-, ν_z, and ν_+ are the magnetron, axial, and modified cyclotron frequencies of the particle in the

Penning trap. Since precise measurements of ν_c are necessary for both charge-to-mass ratio and g-factor measurements, we need detectors to precisely determine the different oscillatory frequencies of a particle in our trap.

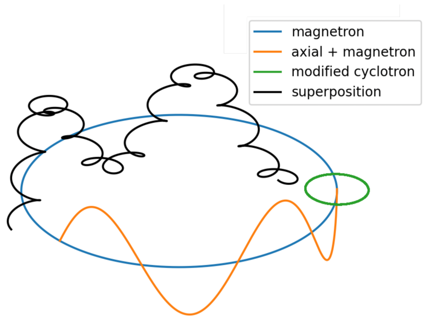

Figure 2: The three modes of oscillation of a particle in a Penning trap.

1.2 Particle Detection

Non-destructive particle detection is performed using the detector setup shown in Figure 3. A particle oscillating in the Penning trap produces an image current i_p, which flows through an RLC resonator and then a cryogenic low-noise amplifier. When a thermalized particle's oscillatory frequency is matched to the detector's resonance frequency it can be detected as a dip in the resonance peak produced by the detector. The Q-factor of the detector's resonator is determined by the following equation:

$$Q = \frac{R_{eff}}{2\pi\nu_0 L}$$

where R_{eff} is the effective resistance of the detector, ν_0 is the resonator's resonance frequency, and L is the resonator's inductance. Energy is removed from the particle by the detector at a rate determined by the cooling time constant:

$$\tau = \frac{m}{R_{eff}} \frac{D^2}{q^2}$$

where m is the particle mass, D is a trap specific length, and q is the particle charge. Another important value for the detector is the SNR:

$$\text{SNR} \approx \frac{\sqrt{4k_B T R_{eff}}}{e_n}$$

where T is the resonator temperature and e_n is the equivalent input noise of the amplifier. More details on the detection mechanism as well as a derivation of the above equations can be found in Chapter 3 of [3].

The detector's amplifier circuit is shown in Figure 4. It consists of two field effect transistors

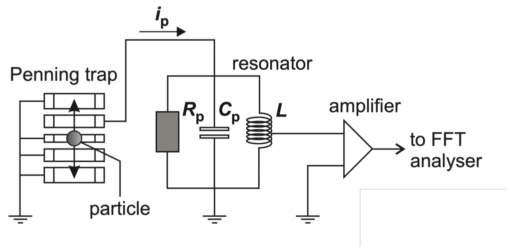

Figure 3: The non-destructive particle detection system. Reproduced from [3].

(FETs), the first acting as a common-source amplifier and the second acting as a source follower. Each of the DC terminals are connected to the circuit through a low-pass RC filter, while the input and output terminals are connected through high-pass RC filters.

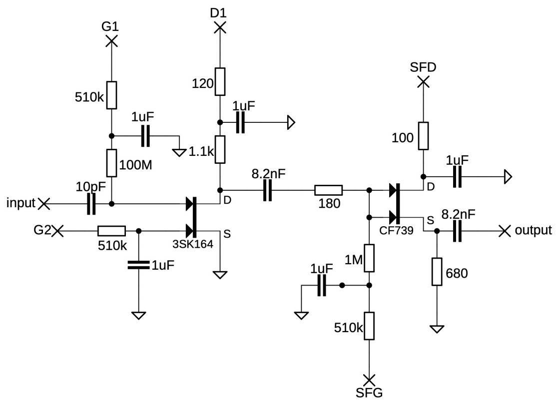

Figure 4: The amplifier circuit.

Each Penning trap BASE-STEP experiment is equipped with two detectors: an axial detector and a cyclotron detector. The axial detectors are responsible for the detection of a particle's axial motion as well as the detection of magnetron motion through sideband coupling. The cyclotron detectors, which can also be used for direct particle detection, are typically used to cool the particle's cyclotron motion. While the axial frequency can be tuned by changing the electric quadrupole potential inside the trap, it is not possible to easily tune the cyclotron frequency as the axial magnetic field is produced by a superconducting magnet. Thus the cyclotron detectors are equipped with varactors – reverse-biased diodes that act as voltage tunable capacitors – to tune their resonance frequency to match the frequency of the particle.

Currently, the two cyclotron resonators in the BASE-STEP trap system are highly coupled, as shown in Figure 5, which distorts their frequency responses. This has a negative affect on both the detectors' cooling time constants τ and their signal to noise ratios (SNRs). In order to combat this interference, varactors are used to tune the resonance frequencies of the two detectors apart from one another. The current detectors have a tuning range of ~150kHz and ~80kHz, which is not enough to reduce the effects of resonator coupling. This summer, I have been tasked with developing and characterizing a new detector setup and a more robust varactor board to both increase the possible tuning range and decrease the detector's cooling time constant τ for more efficient trap operation.

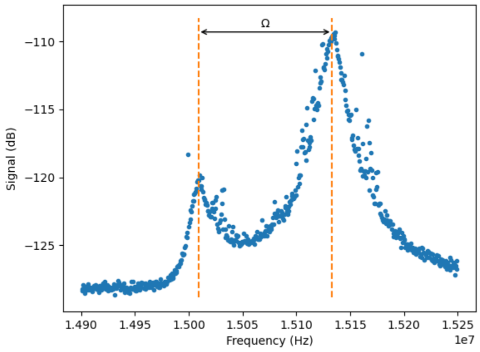

Figure 5: The coupling of BASE-STEP's two cyclotron detectors. Ω is the Rabi frequency of the coupled system.

2 Detector Assembly

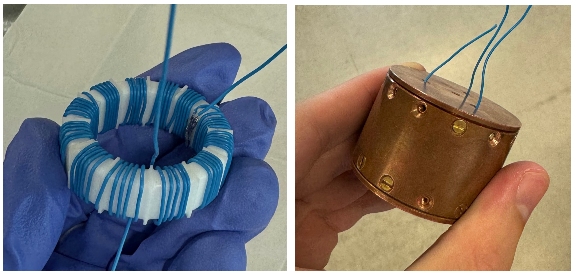

Figure 6: The assembled resonator.

As mentioned above, the detector setup consists of three main components: the resonator, the amplifier, and the varactor circuit. The resonator consists of a PTFE-insulated Cu wire coiled around a toroidal PTFE core placed into a Cu housing, as shown in Figure 6. The inductance of the resonator can be calculated from its dimensions using the following formula:

$$L = \frac{\mu N^2 H \ln\left(\frac{b}{a}\right)}{2\pi}$$

where N is the number of turns in the coil, H is the height of the toroid, b is the outer radius of the toroid, a is the inner radius of the toriod, and μ is

H	b	a	N
11 ± 1mm	18 ± 1mm	12 ± 1mm	62.5

Table 1: The geometry of the assembled resonator. Uncertainty in the dimensions is due to tightness of the wire winding around the resonator core.

the permeability of the core material. Table 1 summarizes the assembled resonator's geometry. These measured values give us an expected coil inductance of $L = 3.5 \pm 0.9$µH.

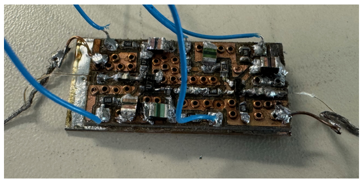

Figure 7: The assembled amplifier.

The assembled amplifier PCB is shown in Figure 7. A Sony 3SK164 Dual-Gate GaAs MESFET was used for the common-source amplifier, and a Siemens CF739 Dual-Gate MESFET was used for the source follower. These two FETs were chosen due to their low noise at low operating temperatures.

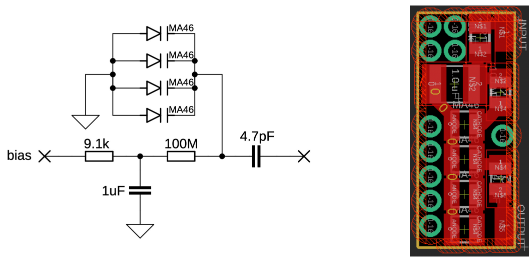

Figure 8: The varactor circuit and PCB design.

The new varactor circuit is shown in Figure 8. It consists of four MACOM MA46H072 varactors connected to a biasing terminal through a low-pass RC filter. The tunable varactor capacitance can be connected to the detector system through the varactor board's second terminal, which is preceded by a filtering capacitor to remove the biasing voltage. The assembled varactor PCB is shown in Figure 9.

3 Detector Characterization

The resonator was characterized to determine its inductance L, capacitance C, and quality factor Q. L and C were determined by measuring the resonator's frequency response with and without a capacitance C' parallel to the resonator. The following two formulas for the resonance frequency with and without the parallel capacitance can be used to determine L and C:

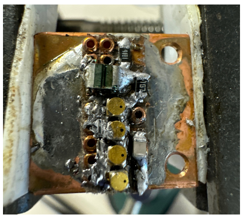

Figure 9: The assembled varactor board.

$$\nu_0 = \frac{1}{2\pi\sqrt{LC}} \qquad \nu_0' = \frac{1}{2\pi\sqrt{L(C+C')}}$$

The Q-factor can be determined by measuring the resonance frequency and the -3dB width $\Delta\nu$ of the resonance peak using the following approximation for large values of Q:

$$Q \approx \frac{\nu_0}{\Delta\nu}$$

The amplifier circuit was characterized to determine its gain G and equivalent input noise e_n as a function of the applied gate 1 and gate 2 voltages, G_1 and G_2. Gain measurements were done by measuring the amplifier's S_{21} parameter on a network analyzer. Measurements of e_n were performed by first connecting a 50Ω terminator to the amplifier's input terminal, then feeding the amplifier's output through an Mini-Circuits ZFL-500LN amplifier, and finally reading the output noise signal a_n with a signal analyzer. The following equation can be used to determine the equivalent input noise from a_n:

$$e_n = \frac{a_n}{GG_{ZFL}}$$

where G_{ZFL} is the gain of the ZFL-500LN amplifier. More details on both the resonator and amplifier characterization can be found in Chapter 6 of [3].

Measurements were also done to determine a good working point for the detector setup in terms of the gate voltages G_1 and G_2. The Miller effect causes an unwanted feedback between the amplifying FET's gate and drain, which both shifts and stretches/squishes the detector's resonance peak. By careful tuning of G_1 and G_2, we can minimize the effects of this feedback while still maintaining reasonable values for the detector's Q-factor and gain. Specifically, detector working points were found by measuring of ν_0, G, and Q as a function of G_1 and G_2 by looking at the complete detector setup through a network analyzer.

Finally, the tuning range of the varactor circuit in the complete detector setup was measured. In the completed setup, the varactor circuit was placed in parallel with the resonator coil to maximize the tuning range. Values of both ν_0 and Q were measured as a function of the varactor bias voltage V_{bias} to determine the tuning range and look for an effect on the detector's Q-factor.

Measurements were done at both room temperature (RT) and low temperature (11K) to simulate the ~4K operating temperature of the BASE-STEP experiment. Low temperature measurements were performed inside of a GM cooler cryostat.

4 Results

The resonator was measured to have inductance $L = 3.7 \pm 0.1$µH, which clearly matches the expected value of $L = 3.5 \pm 0.9$µH, and capacitance $C = 8.2 \pm 0.2$pF. These values correspond to an unloaded resonance frequency of $\nu_0 = 29$MHz. The Q-factor was measured at RT to be ~170 and at 11K to be ~750. The resonator's frequency response at both RT and 11K can be seen in Figure 10. The results of the amplifier gain and equivalent input noise measurements at RT and 11K are shown in Figure A.1 and Figure A.2. Good working points for the detector setup at RT and 11K were found to be $G_1 = -1.55$V, $G_2 = 0.93$V and $G_1 = -1.03$V, $G_2 = -0.45$V, respectively. The plots of the gain, equivalent input noise, and resonance frequency as a function of gate voltages used to determine these values are given in Figure B.1 and Figure B.2. The tuning range of the varactor board was found to be ~565kHz at RT and ~540kHz at 11K, which can be seen in Figure C.3. The varactor bias voltage V_{bias} was also found to have a negligible effect on the detectors Q-factor, which is shown in Figure C.4. A summary of the detector's performance is given in Table 2.

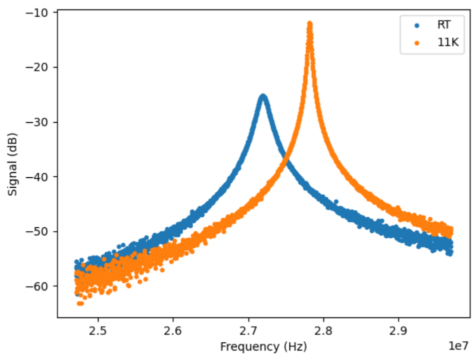

Figure 10: Frequency response of the resonator at both RT and 11K

5 Conclusion

The detector setup's values of L, Q, and e_n correspond to a 25% reduction in the cooling time

	RT	11K
G_1,G_2	-1.55V,0.93V	-1.03V,-0.45V
ν_0	~17.8MHz	~16.8MHz
Amplitude	14.0dB	19.4dB
Q	105.998	609.834
e_n	~4nV/$\sqrt{\text{Hz}}$	~2nV/$\sqrt{\text{Hz}}$
Tuning range	~565kHz	~540kHz

Table 2: A summary of the detector's performance at both the RT and 11K working points.

constant τ when compared to the current detectors, which will result in more efficient trap operation. The measured values also correspond to a high approximate SNR of ~16dB. Furthermore, the new varactor board almost quadrupled the resonance frequency tuning range compared to that of the old detectors. Also, since the new detector increases the resonator inductance from the old detector's inductance of $L = 2.7$µH, we expect a drop in the detector's Q-factor. Luckily, the new detector's Q-factor is still quite high, with only a roughly 10% reduction when compared to the old detector. Now that the new cyclotron detector has demonstrated the desired improvements, it is ready to be installed in the BASE-STEP trap system during the next round of upgrades.

Acknowledgements

I would like to thank my supervisor Dr. Christian Smorra, as well as his graduate students Marcel Leonhardt and Daniel Popper, for their guidance and assistance on this project. My thanks also goes out the the University of Michigan REU coordinators, Dr. Myron Campbell, Dr. Junjie Zhu, and Dr. Steven Goldfarb, as well as the NMS CERN Summer Student Coordinator, Ernest Zakrzewski, for giving me the opportunity to come to CERN for the summer. This work was supported by NSF grant number 2243608.

References

[1] V. Alan Kostelecky and Robertus Potting. CPT and strings. *Nucl. Phys. B*, 359:545–570, 1991.

[2] C. Smorra, F. Abbass, D. Schweitzer, M. Bohman, J. D. Devine, Y. Dutheil, A. Hobl, B. Arndt, B. B. Bauer, J. A. Devlin, S. Erlewein, M. Fleck, J. I. Jäger, B. M. Latacz, P. Micke, M. Schiffelholz, G. Umbrazunas, M. Wiesinger, C. Will, E. Wursten, H. Yildiz, K. Blaum, Y. Matsuda, A. Mooser, C. Ospelkaus, W. Quint, A. Soter, J. Walz, Y. Yamazaki, and S. Ulmer. BASE-STEP: A transportable antiproton reservoir for fundamental interaction studies. *Review of Scientific Instruments*, 94(11):113201, 11 2023.

[3] Hiroki Nagahama. *High-Precision Measurements of the Fundamental Properties of the Antiproton.* PhD thesis, Tokyo U., 2017.

Appendix A Amplifier Characterization

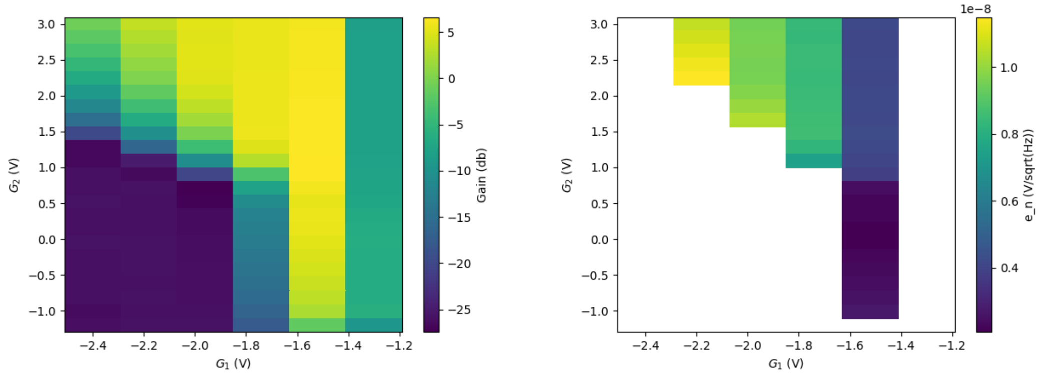

Figure A.1: Gain and e_n as a function of the gate voltages G_1 and G_2 at RT. Points with to negative gain were emitted from the plot of e_n.

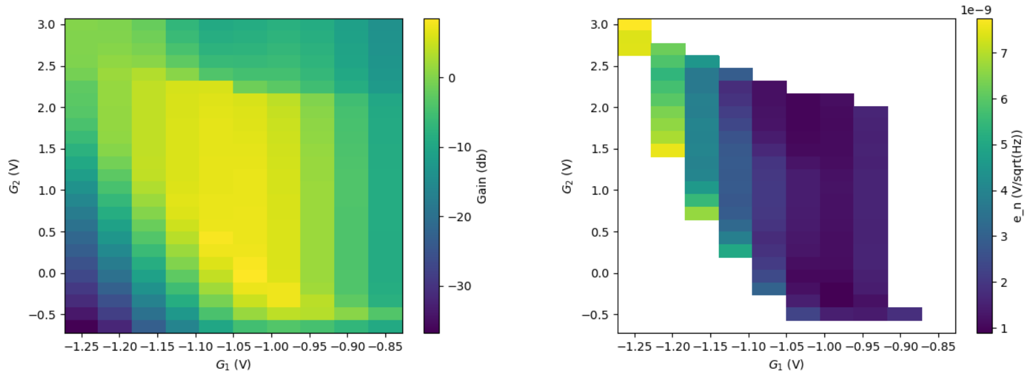

Figure A.2: Gain and e_n as a function of the gain voltages G_1 and G_2 at 11K. Points with to negative gain were emitted from the plot of e_n.

Appendix B Miller Effect Characterization

The measurement results from the complete detector characterization are shown in Figures B.1 and B.2. Detector working points can determined by looking for gate voltages that result in neither a stretched or squished resonance peak. This was done by picking a point that has both a Q-factor in the middle of the possible range of values and a high signal amplitude. As can be seen in Figure B.2, results changed between the coarse and fine scan. This is believed to be the result of poor amplifier thermalization within the cryostat.

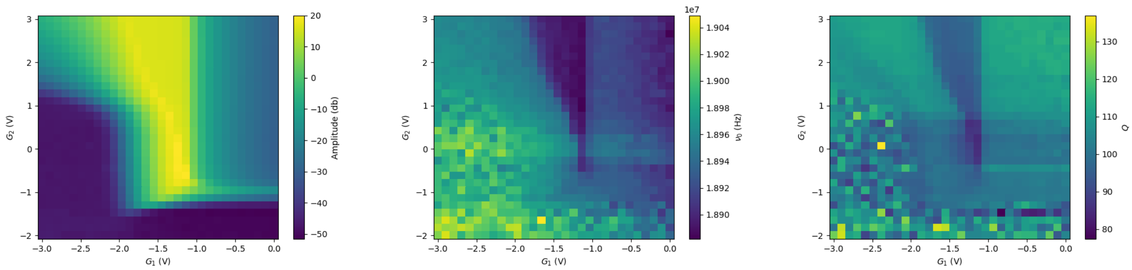

Figure B.1: Results from the complete detector setup measurements to determine a RT working point.

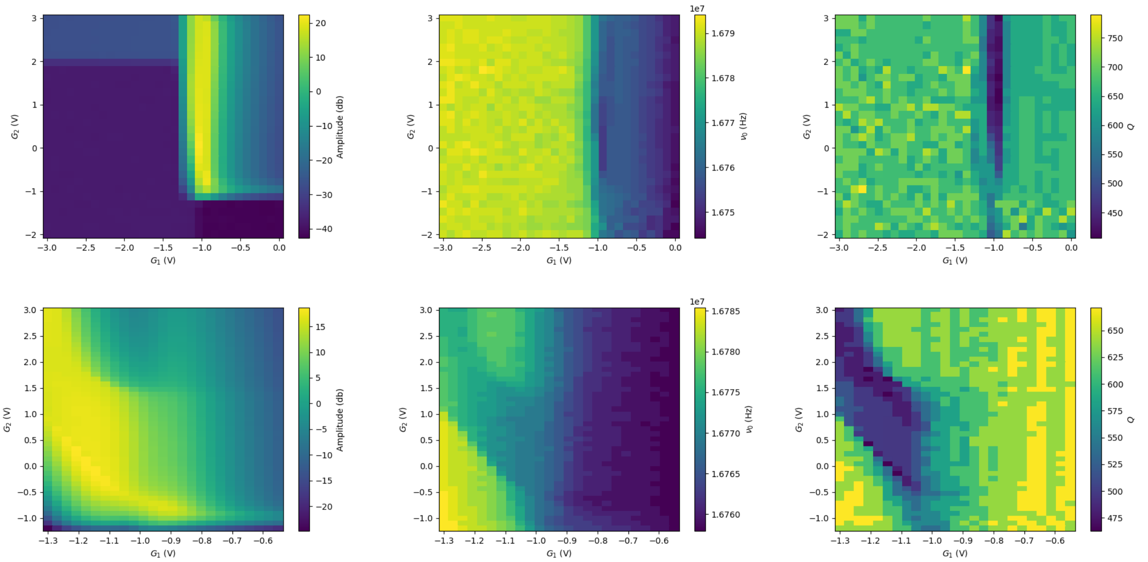

Figure B.2: Results from the complete detector setup measurements to determine an 11K working point. The first set of plots are from a course scan over the possible gate voltages and the second is from a finer scan.

Appendix C Varactor Characterization

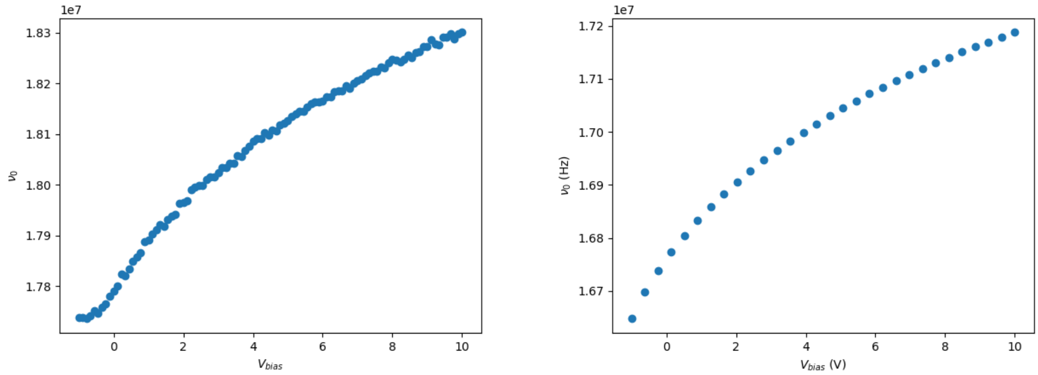

Figure C.3: Detector resonance frequency vs varactor bias voltage at both RT (right) and 11K (left).

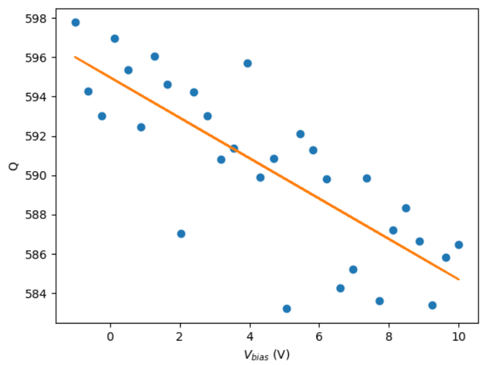

Figure C.4: Detector Q-factor vs varactor bias voltage at 11K.